Received: 19 July 2021 | Revised: 20 August 2021 | Accepted: 23 August 2021

DOI: 10.1002/pol.20210565

RESEARCH ARTICLE

JOURNAL OF POLYMER SCIENCE WILEY

Elucidating the impact of side chain dispersity on the assembly of bottlebrush polymers at the air-water interface

Nduka D. Ogbonna[1] | **Michael Dearman**[1] | **Bhuvnesh Bharti**[1] | **Andrew J. Peters**[2] | **Jimmy Lawrence**[1]

[1]Department of Chemical Engineering, Louisiana State University, Baton Rouge, Louisiana, USA

[2]Department of Chemical Engineering, Louisiana Tech University, Ruston, Louisiana, USA

Correspondence
Jimmy Lawrence, Department of Chemical Engineering, Louisiana State University, Baton Rouge, LA 70803, USA.
Email: jimmylawrence@lsu.edu

Andrew Peters, Department of Chemical Engineering, Louisiana Tech University, Ruston, LA 71272, USA.
Email: apeters@latech.edu

Funding information
Louisiana State University start-up; Louisiana Board of Regents, Grant/Award Number: RD-A-07, RD-A-18; Louisiana Tech University start-up; BASF Living Sustainability Laboratory Program; National Science Foundation, Grant/Award Number: CBET-2038305; Louisiana Optical Network Infrastructure

Abstract

The synthesis of bottlebrush polymers with discrete side chains, their surface pressure isotherm measurements, and thin film molecular dynamics simulations are reported. Our results show that monolayers of bottlebrushes with discrete side chains achieve higher packing densities and exhibit previously unknown, distinct phase transitions that are unseen in their disperse counterparts. The combination of experimental findings and simulation results show that shape-defined bottlebrush polymers can advance structure–property relationship studies of branched polymers and the theoretical descriptions of polymer monolayer self-assembly.

KEYWORDS

bottlebrush polymers, discrete side chains, Langmuir–Blodgett, precision polymers, self-assembly

1 | INTRODUCTION

Interest in the precise control of polymer structure and properties, akin to the precision commonly found in biological systems (e.g. DNA and polypeptides), has driven polymer chemists and material scientists to develop versatile and efficient methods for preparing well-defined and structurally complex materials.[1–3] For example, monodisperse (discrete) materials have been synthesized directly via stepwise iterative coupling and, recently, isolated in large quantities from disperse mixtures with automated column chromatography.[4–12] Utilizing these methods, many research groups have reported scalable and versatile control of polymer dispersity and molar mass distribution, yielding previously unknown length-dependent properties and providing invaluable fundamental insights.[9–19] For example, Meijer and coworkers showed that discrete ABA-type amphiphilic triblock co-oligomers self-assemble in water with higher structural regularity (nanofibers/2D sheets) and crystallinity than their disperse counterparts.[16] However, this level of precise control and insight has been vastly limited to traditional linear polymers.

In the regime of branched polymeric soft materials, only dendrimers have attained a similar level of control as their linear counterparts.[20–22] However, the chemical versatility of dendrimers and their widespread adoption are often limited by exhaustive stepwise synthesis and post-synthetic modifications to reach the targeted structure and functionalities. In contrast, the advent of robust controlled polymerization and highly efficient coupling techniques has dramatically eased the preparation of

Nduka D. Ogbonna and Michael Dearman equally contributed to this work.

multifunctional-branched polymers with bottlebrush-like morphologies.[23–25] These bottlebrush polymers differ from typical linear structures, which are synthesized by joining small-molecule monomers. Instead, bottlebrush polymers are prepared from larger, linear polymers using *grafting-from*, *grafting-to*, or *grafting-through* methods and consist of a primary chain (backbone) from which secondary chains (side chains) extend.[23,24] However, the structural complexity of bottlebrush polymers, coupled with their lack of precision in synthesis relative to dendrimers, is accompanied by an exponential increase in structural variation and inherent loss of control, specifically with respect to the uniformity of the bottlebrush side chains.[26] These characteristics are the reason soft matter like bottlebrush polymers have not achieved the same level of precision as their linear or dendrimer counterparts, leaving the effects of side chain dispersity an open question. Addressing the structural precision challenge of bottlebrush polymers will narrow the gap between real-world samples and theoretical models, and ultimately improve our understanding of their structure–property relationships.

At the outset of our studies, we focused on preparing fully grafted bottlebrush polymers with side chain length that can be systematically varied. The *grafting-through* ring-opening metathesis polymerization (ROMP) synthesis method developed by Grubbs and coworkers guarantees full grafting density and removes the concern of side chain density variations and other topological defects.[27] Our primary aim was to understand the difference between bottlebrush polymers with topologically discrete, uniform side chains and conventional material with disperse side chain architectures. Provided the syntheses were successful, we envisioned surface pressure isotherm measurement of Langmuir–Blodgett (LB) monolayers to be a powerful strategy for probing the physical behavior and intermolecular interactions of shape-defined bottlebrushes. Surface pressure isotherms are determined by the molecular architecture of polymers and their orientations at the air–water interface, and are sensitive enough to distinguish polymer tacticity.[28,29] In addition, the unique feature of constraining material interactions at the interface, wide material scope, and low material requirements make the LB technique particularly well suited for designing our studies.

To study the impact of structural parameters, we prepared bottlebrush polymers with average four side chain repeat units ($N_{SC} = 4$) and an average backbone length of 30 repeat units ($N_{BB} = 30$). *t*-Butyl acrylate (tBA)-based macromonomer was chosen because the isolation of discrete tBA oligomers and their length-dependent physical properties at monodisperse limit were well studied.[11,30] Furthermore, readily available discrete oligo(tBA) libraries prompted us to design a unique diblock bottlebrush block copolymer from dimeric and octameric macromonomers ($N_{SC} = 4$ and $N_{BB} = 30$) for comparative studies.

2 | EXPERIMENTAL

2.1 | Materials and methods

All reactions were carried out under an inert atmosphere in oven dried glasswares. All reagents were purchased from Sigma-Aldrich/millipore and used without further purification, unless stated otherwise. Copper (II) bromide (>99%) and ethyl vinyl ether (99%) were purchased from Acros Organics. *tert*-Butyl acrylate (Alfa Aesar, 99%) was passed through a plug of neutral alumina to remove inhibitors prior to use. Solvents for chromatographic separation were purchased from VWR chemicals and used without further purification. Deuterated chloroform (99.8%) was purchased from Cambridge Isotope Laboratories. Deionized water was obtained from an ELGA Purelab Flex commercial purifier. Grubbs 3rd generation (G3) catalyst was synthesized according to literature.[31]

Reactions were monitored using silica gel 60G F_{254} TLC plates (EMD Millipore) and visualized under UV illumination or stained with bromocresol green or potassium permanganate. Silica-gel chromatography was performed using 60 Å pore silica gel for manual column and automated separation was performed using a Biotage Isolera One unit equipped with an evaporative light scattering detector (ELSD, Teledyne ISCO 340CF, SNAP/SNAP Ultra cartridges). High-resolution polymer purifications were performed using a recycling size-exclusion chromatography instrument (rSEC, LaboACE LC-5060) equipped with a cross-linked polystyrene/divinylbenzene column (PS/DVB, JAIGEL series), eluting with chloroform.

2.2 | Characterizations

^{1}H and ^{13}C NMR spectra were recorded with Bruker Avance III 400 and 500 MHz spectrometers at 298 K. Chemical shifts (δ) are given in parts per million (ppm) and referenced using a deuterated solvent signal. Number average molecular weight (M_n) and dispersity ($Đ$) of polymer samples were determined using size exclusion chromatography (SEC) (TOSOH HLC-8320GPC) equipped with a cross-linked polystyrene/divinylbenzene column (TSKgel superH5000, polystyrene calibration standard, THF eluent) and a Wyatt Dawn EOS multi-angle light scattering (MALS) detector ($\lambda = 658$ nm, Astra 6 software).

MALDI-TOF-MS spectra were collected using a Bruker UltrafleXtreme tandem time-of-flight mass

spectrometer in positive reflectron mode. Unless otherwise stated, samples for MALDI analysis were prepared by mixing with a 2,5-dihydroxybenzoic acid (DHB)/sodium trifluoroacetate (Na-TFA) matrix, and the mixture deposited on a Bruker MTP 384-polished steel target plate. MALDI ToF data were processed using Bruker FlexAnalysis software.

FTIR spectra were collected on a Bruker Tensor 27 system equipped with a room temperature DTSG detector, a mid-IR source (4000–400 cm^{-1}), a KBr beam splitter, and a Pike Miracle single bounce attenuated total reflectance (ATR) ZnSe single crystal cell. The spectral resolution was set to 4 cm^{-1} and 32 scans were taken for each sample. FTIR data for all samples were processed using Bruker OPUS software suites.

2.3 | Synthesis of oligo(*t*-butyl acrylate) using cu(0)-RDRP (reversible deactivation radical polymerization)

Following literature procedures,[32] copper wire (8 cm) was immersed in HCl for 20 min, rinsed with DI water and acetone, and dried before use. To a 40 ml oven-dried vial, copper(II) bromide ($CuBr_2$) (0.05 equiv.), tris [2-(dimethylamino)ethyl] amine (Me_6TREN) (0.2 equiv.), and trifluoroethanol (TFE) were added, and the mixture sonicated for 10 min. *tert*-Butyl acrylate monomer (tBA) (3 equiv.), *tert*-butyl bromoisobutyrate initiator (tBiB) (1 equiv.), and a stir bar wrapped with the acid-etched copper wire were added to the vial, and the mixture was purged with Ar for 20 min. The polymerization was run at room temperature while stirring for 2 h under an inert atmosphere, and the reaction was terminated by quenching with liquid nitrogen and exposing to the ambient atmosphere. The resulting product was diluted with chloroform, passed through a neutral alumina plug, and reduced in vacuo to obtain crude disperse oligomers.

2.4 | Synthesis of ω-norbornenyl oligo (*t*-butyl acrylate) macromonomer

To an oven-dried vial containing oligo *tert*-butyl acrylate (otBA) (1 equiv.), dimethylformamide (DMF) was added to dissolve the oligomer. *Exo*-5-Norbornene-2-carboxylic acid (1.2 equiv.) was added, followed by dropwise addition of 1,8-diazabicyclo[5.4.0]undec-7-ene (DBU) (2 equiv.). The reaction proceeded at room temperature while stirring for ~24 h.[33] The mixture was then extracted with EtOAc, and the combined organic extract was washed with brine, dried over anhydrous sodium sulfate, and filtered. Excess solvent was reduced in vacuo. The crude product was purified using column chromatography (10% EtOAc/Hexane) to obtain the desired disperse macromonomer (yield: 86%). A portion of the disperse macromonomer (e.g., average 4-mer, 7 g) was separated using a combination of automated flash chromatography and recycling SEC to obtain a library of synthetically pure discrete macromonomers (e.g., 2-mer to 8-mer).[11]

2.5 | Synthesis of bottlebrush polymers

Grafting-through ROMP was employed for the synthesis of bottlebrush polymers. Bottlebrush polymers prepared from disperse- and discrete macronomonomers will be referred to as BB-n and PBB-n, respectively, with *n* representing the number of side chain repeat units. For **BB-4**, **PBB-4**, **PBB-2**, and **PBB-8**, the macromonomer (30 equiv.) was dissolved in DCM and degassed with Ar for 20 min. A degassed DCM solution of G3 (1 equiv.) was injected into the mixture to initiate the polymerization. The mixture was stirred at room temperature for ~1 h and quenched with excess ethyl vinyl ether.[27] The bottlebrush diblock copolymer (**PBB-2/8**) was synthesized by sequential addition of macromonomers.[34] The second macromonomer was injected following > 99% conversion of the first macromonomer.

2.6 | Langmuir–Blodgett isotherm measurement

The surface pressure isotherms of the bottlebrush polymer samples were measured using a Langmuir–Blodgett trough system with two movable PTFE barriers and a platinum Wilhelmy plate.[35,36] For each LB experiment, the trough was cleaned with DI water, rinsed with anhydrous ethanol, and air-dried. This cleaning process was repeated 3 times to eliminate all impurities, and contaminant removal was confirmed through measuring the isotherm of pure water. The temperature of the aqueous substrate was maintained using a circulating water bath. **The bottlebrush polymer sample (e.g., BB-4)** was spread at the air–water interface by depositing 70 μl of a 0.03 mg/ml chloroform solution to form a 40 cm^2 closely packed monolayer. The chloroform was allowed to evaporate over 10 min, and LB trough barriers were compressed at a rate of 5 mm/min. For each sample, the isotherm measurement was repeated at least twice, and similar procedures were followed for all bottlebrush samples.

2.7 | Coarse-grained molecular dynamics simulation

A two-dimensional Kremer-Grest like model[37] was used to simulate the packing of the bottlebrush polymers in

the Langmuir–Blodgett isotherm experiments using Langevin dynamics. A single bead was used to model each backbone monomer and each of the side chain monomers. The two-dimensional nature of the simulation was intended to model polymers trapped at the air-water interface, and it is important to note that it forces all molecules to lay parallel to the interface and does not allow any vertical chains, even when under intense pressure.

Reduced units were used where the length unit = $\mathcal{D}$ = diameter of a polymer bead, energy unit = $\mathcal{E}$ = interaction energy between beads, and mass unit = $\mathcal{M}$ = mass of a polymer bead. Other units are derived from these units as appropriate. For example, time is in units of:

$$\tau = \sqrt{\frac{\mathcal{M}\mathcal{D}^2}{\mathcal{E}}} \tag{1}$$

and velocity is in units of:

$$v = \mathcal{D}/\tau \tag{2}$$

These reduced units can be mapped onto real units by picking a set of values for $\mathcal{D}$, $\mathcal{M}$, *and* $\mathcal{E}$. For example, the length unit can be set to the cube root of the molar volume divided by Avagadro's number. Taking a molar volume of 128.2 $Å^3$/mol (from a density of 1.00 g/cm^3)[38] gives $\mathcal{D} = 5.97$ Å. This can be used to compare the simulated results with experimental findings.

All polymer beads were identical and interacted via a Lennard-Jones potential:

$$U_{LJ} = \begin{cases} 4\varepsilon\left[\left(\frac{\sigma}{r}\right)^{12} - \left(\frac{\sigma}{r}\right)^{6}\right] & r < r_{cut} \\ \\ 0 & r \geq r_{cut} \end{cases} \tag{3}$$

with $\sigma = 1$, $\varepsilon = 1$, and $r_{cut} = 3$. The bonds were modeled as harmonic:

$$U_{bond} = k_{bond}(r - r_0)^2 \tag{4}$$

with $k_{bond} = 100$ and equilibrium distance $r_0 = 1$. A harmonic angle potential was applied to every set of 3 bonded beads:

$$U_{angle} = k_{angle}(\theta - \theta_0)^2 \tag{5}$$

with $k_{angle} = 30$ and equilibrium angle $\theta_0 = 1.95477\,rad$. Langevin dynamics using the software HOOMD-blue[39,40] with a reduced temperature of $T^* = 3$ was used. A timestep of 0.01 was use with $\gamma = 0.5$ and the seed for the random number generator was set using /dev/random.

To build the simulation for the discrete and diblock topologies, a single molecule with 30 backbone beads was built in a 120 × 120 square and minimized using HOOMD-Blue's FIRE minimizer. For the discrete topology, each side chain consisted of 4 beads, while for the diblock topology the first 20 side chains were 2 beads long, and the last 10 side chains were 8 beads long. The lengths of side chains from the disperse topology were independently generated from MATLAB's "randi" random number generator[41] using a uniform distribution between 0 and 8 such that the average would be 4 beads on each side chain. Every side chain length from 0 to 8 is equally likely to occur. To account for the possibility of different distributions resulting in different isotherms because of the small number of molecules, 10 different disperse builds (each with 100 molecules) were run. The run-to-run and build-to-build variation is negligible (Figure S9). For the diblock and discrete topologies, the molecule was then run under Langevin dynamics for 1000 timesteps, then replicated 10 times in each dimension. For the disperse topology, the structures of all 100 molecules were minimized simultaneously. At this point, the molecules are far enough away that they do not interact.

To simulate Langmuir–Blodgett style isotherms, the system was then shrunk (the box dimension was varied linearly with time) while running Langevin dynamics over 100,000 timesteps to 120 × 120 (400 units of area per molecule, 2.6666 units of area per bead), then slowly shrunk over 10,000,000 time steps to 122.47 × 122.47 (150 units of area per molecule, 1 unit of area per bead). The pressure and energy were logged every 100 time steps, and the positions of the beads were saved every 10,000 time steps.

3 | RESULTS AND DISCUSSION

3.1 | Synthesis and characterization of macromonomers and bottlebrush polymers

We synthesized norbornene-functionalized oligo(*t*-butyl acrylate) macromonomers using Cu(0)-RDRP and DBU-catalyzed esterification.[33] The oligomerization of *t*-butyl acrylate gave excellent conversions, satisfactory yield, and excellent chain-end fidelity (see Figure S1). The chemical structures of macromonomers and bottlebrush polymers synthesized in this study are depicted in Scheme 1, and their structural parameters summarized in Tables 1 and 2. We opted to prepare ω-norbornenyl-

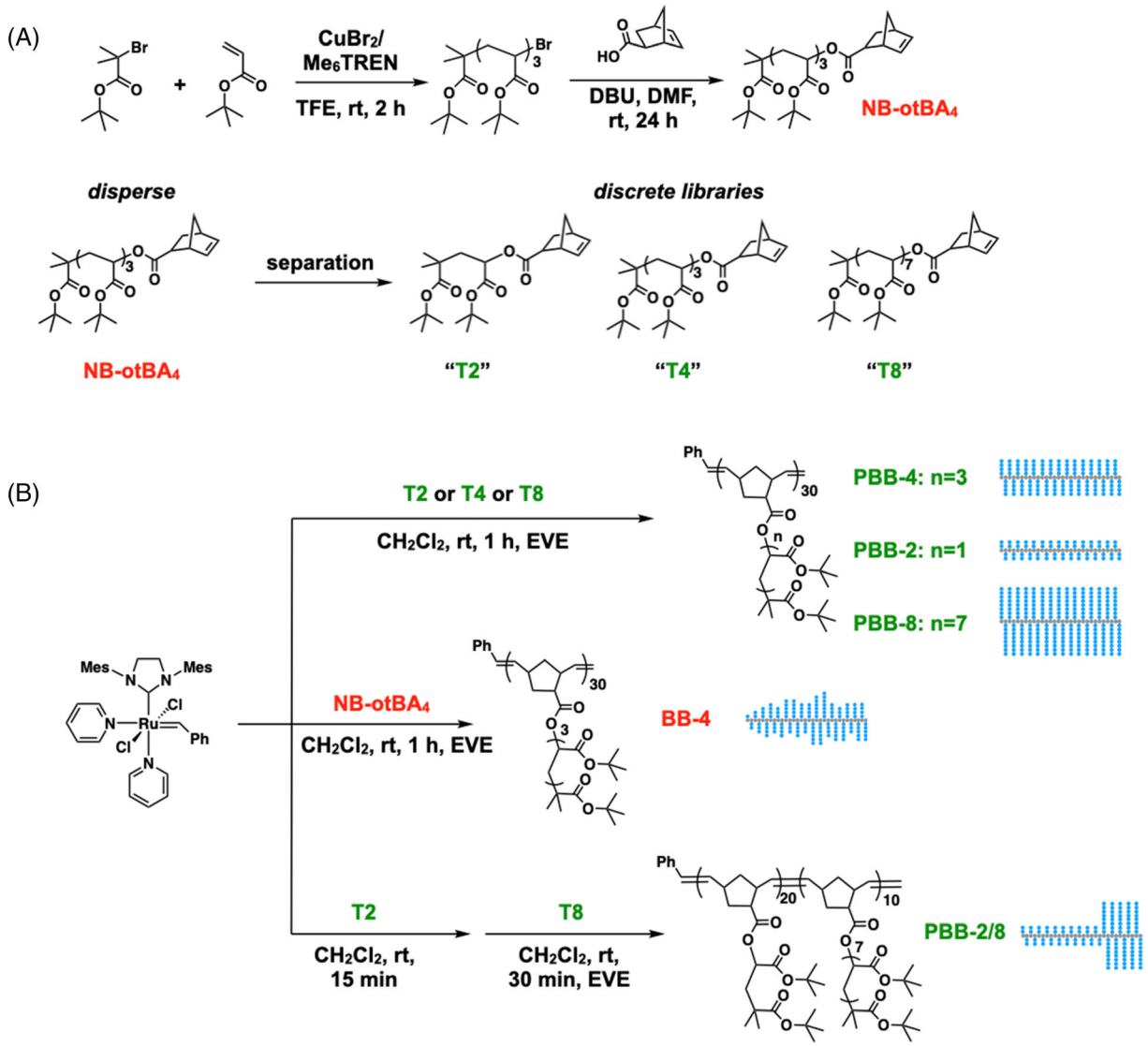

SCHEME 1 (A) Synthesis of bromine-terminated oligo(*t*-butyl acrylate) via cu(0)-RDRP and ω-norbornenyl oligo(*t*-butyl acrylate) macromonomer via nucleophilic substitution of the bromine chain end. (B) Synthesis of the bottlebrush polymers used for this study via *grafting-through* ROMP

macromonomers following the strategy reported by Xia and co-workers,[27] to avoid contaminations from chain-chain coupled compounds commonly seen in the synthesis of α-norbornenyl macromonomers.

Through this modular chain-end modification strategy, pure disperse, and discrete macromonomers were obtained in relatively high yield (> 85%). ^{1}H NMR analysis confirms chain-end conversion by the downfield shift of the chain-end methine proton from 4.1 to 4.8 ppm and the appearance of the norbornenyl cyclic alkene proton at 6.1 ppm (Figure S1). MALDI-ToF analysis shows an increase in m/z by 58 amu, further confirming the quantitative replacement of the bromine chain-end with the norbornenyl group (Figure S3). Following chromatographic separation of the crude macromonomers, the structural purity ($Đ = 1.0$) of the discrete libraries was confirmed via MALDI-ToF mass spectrometry (Figure 1).

The structural homogeneity of these discrete macromonomers allowed us to prepare precision bottlebrush polymers, providing a fundamental understanding of their dynamics, interactions, and orientation at the air-water interface. We found these properties are influenced by the precision bottlebrush polymers' unique geometric architectures. Because the polymer samples were prepared through *grafting-through* ROMP, all samples exhibited a unimodal Gaussian-like distribution with narrow dispersity ($Đ < 1.04$) in their size-exclusion chromatograms (Figure S5). SEC-MALS analysis also confirmed all bottlebrush samples have a similar average backbone length ($N_{BB} \sim 30$).

TABLE 1 Macromonomers used for the bottlebrush polymers synthesis

Entry	Code	Sample[a]	M_n[b] (Da)	$Đ$[b]
1	NB-otBA4	Disperse NB-otBA4	700[c]	1.07[c]
2	T2	Discrete NB-otBA2	408.25	1.00
3	T4	Discrete NB-otBA4	664.45	1.00
4	T8	Discrete NB-otBA8	1176.58	1.00

[a]The number in sample names represent the number of *t*-butyl acrylate repeat units.
[b]Determined using MALDI-ToF.
[c]Determined using SEC-MALS.

TABLE 2 Bottlebrush polymers synthesized in this study

Code	Sample[a]	MM	Conv. (%)[b]	BB $M_{n,theo}$[c] (kDa)	$M_{n,obsd}$[b] (kDa)	$Đ$[b]	N_{BB}[b]	$N_{BB,NMR}$[d]
BB-4	$P(NB\text{-}otBA4)_{30}$	NB-otBA4	> 99	19.9	24.0	1.02	34	36
PBB-4	$P(T4)_{30}$	T4	> 99	19.9	20.3	1.01	30	32
PBB-2/8	$P(T2_{20}\text{-}b\text{-}T8_{10})$	T2 & T8	> 99	19.9	21.7	1.03	32	34
PBB-2	$P(T2)_{30}$	T2	> 99	12.2	14.5	1.01	35	35
PBB-8	$P(T8)_{30}$	T8	> 99	35.3	41.0	1.01	34	33

[a]BB-4 was prepared from disperse macromonomers, and all precision bottlebrush polymers (PBB series) were prepared from discrete macromonomers.
[b]Measured by SEC-MALS. $N_{BB} = M_{n,bottlebrush}/M_{n,macromonomer}$.
[c]$M_{n,theo} = [MM]_0/[G3]_0 \times M_n$ of MM × conversion (%).
[d]Measured from ^{1}H NMR using the chain-end proton signal (6.4 ppm) as a reference.

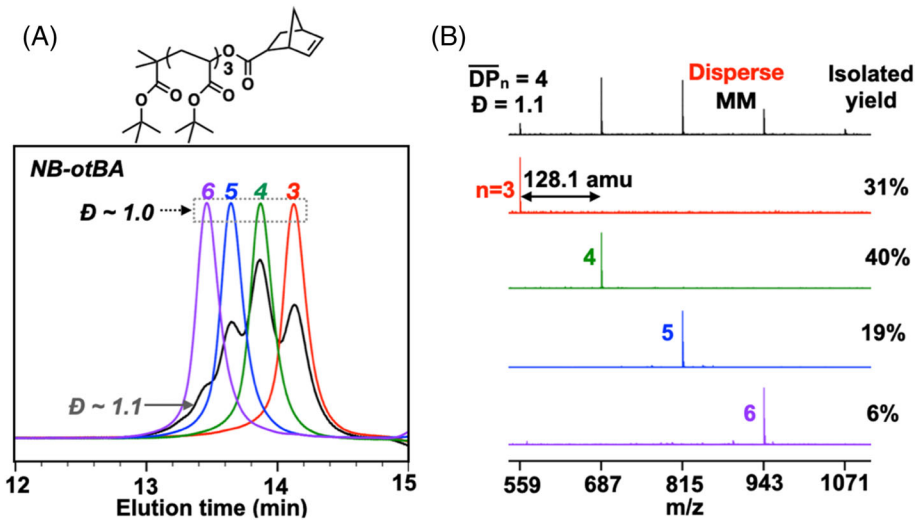

FIGURE 1 (A) SEC (B) MALDI-ToF of the disperse and few discrete libraries used for the bottlebrush synthesis. Red, green, blue, and purple spectra are discrete trimer, tetramer, pentamer, and hexamer, respectively

The structural differences of the bottlebrush polymers were observed by comparing their ^{1}H NMR spectra. Two distinct peaks corresponding to the methine proton were observed for the diblock architecture (one for the dimeric block at 4.83 ppm and the other for the octameric block at 4.73 ppm). This splitting indicates the different environments surrounding these protons. Only a single peak is observed for bottlebrushes with disperse and discrete side chains (Figure 2 and Figure S4).

3.2 | Langmuir–Blodgett monolayer deposition of polymer samples

The packing of the molecules at the interface governs the net surface pressure as determined by LB experiments. For all tested BB polymers, we observe an increase in surface pressure with increasing compression (e.g. closing barriers). This increase in pressure corresponds to an increase in the effective number density of molecules at the interface and resultant changes in the assembled state

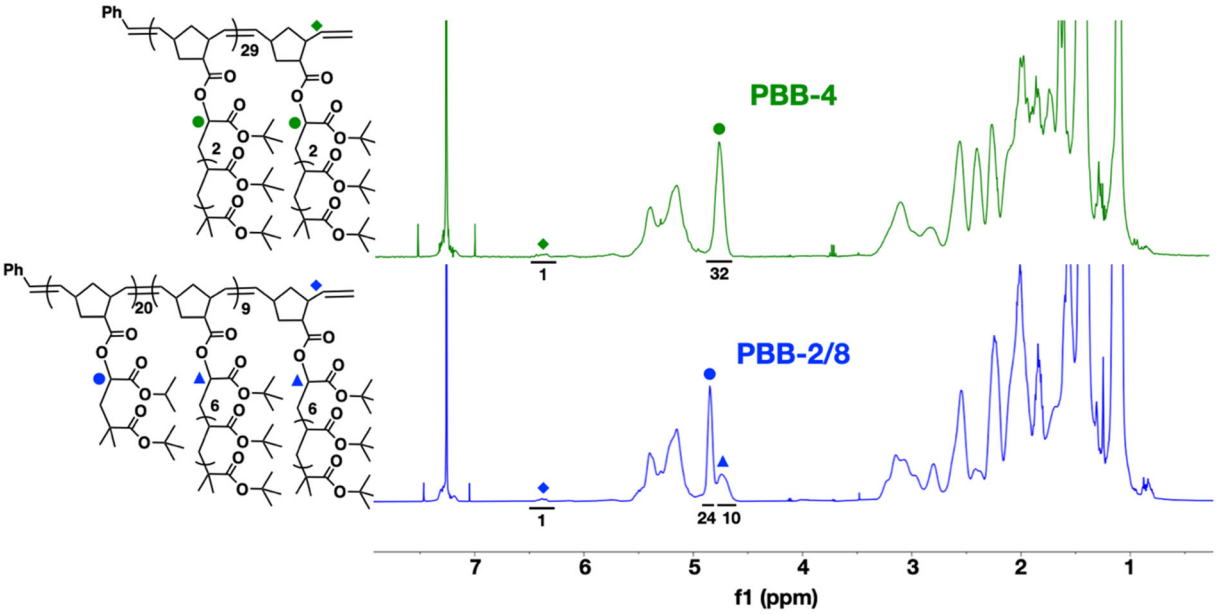

FIGURE 2 Chemical structure and ^{1}H NMR ($CDCl_3$, 500 MHz) spectra of **PBB-4** (green) and **PBB-2/8** (blue). Diamond = chain end proton, green circle = "methine" proton due to tetrameric block, blue circle = "methine" proton due to dimeric block, and blue triangle = "methine" proton due to octameric block

of the molecules. The changes in the assembled state of each BB are dependent on their molecular structure and intermolecular interactions. For each BB polymer, there is a characteristic onset of increased surface pressure ($\prod^*$), which indicates packed molecules at the interface. We find that the value of $\prod^*$ increases at 132, 170, and 195 nm^2/molecule for bottlebrushes with tetrameric discrete, diblock, and disperses, respectively. Given that the chemical nature of the side chains and backbone for all our BB polymers is identical, the observed changes in $\prod^*$ can be attributed primarily to changes in the assembled structures of the polymers upon compression. The onset of increasing $\prod^*$ at a lower area per molecule for discrete tetrameric side chain BB indicates closer packing in comparison to diblock and disperse units. Side chain DP dictates the width of each bottlebrush species, increasing intermolecular distance between macromolecules at higher DP and decreasing for lower DP. The presence of side chain units longer than discrete tetramer in the diblock and disperse side chain bottlebrushes triggers an onset of increasing $\prod^*$ at a molecular area higher than their discrete analogues. The homogeneous width of the discrete side chain bottlebrush induces smaller free volume and hence, a closer packing. Work performed by Xia and coworkers shows self-assembly and formation of macro-structures in bulk polymer melts,[42] indicating similar behavior in 2- and 3-dimensional regimes. From this evidence and a study by Meijer and coworkers,[16] the observed relative packing differences between disperse and discrete side chain bottlebrushes translate to the macroscopic properties of the bulk material. Note that for all tested BB polymers, we do not observe a plateau in the surface pressure, which represents the "pancake" to "brush" transition commonly seen in amphiphilic brush copolymers and other architectures.[43–45] The lack of plateau implies gradual changes in the assembled structures rather than the typical gas-to-liquid-to-solid first-order phase transitions, as observed in compression isotherms for surfactant molecules and silica nanorods.[46] Instead, we observe three distinct periods of stress on the material (Figure 3A). In regime 'i', the bottlebrushes are freely diffusing on the plane (unperturbed). In 'ii', the bottlebrushes form a closely packed film without perturbation to their conformations. This phase appears more distinct for the discrete material. In 'iii', the bottlebrushes are compressed further, presumably triggering some conformational changes or minor side chain–side chain interdigitation.[35,47,48] Absence of the sharp transition from region 'ii' to 'iii' for the diblock and disperse bottlebrush samples is likely due to the disperse side chain topology. Our results indicate that such artificial topological "defects" affect inter-brush interactions and their packing, and this lack of sharp transition for disperse bottlebrush polymers was also reported by Matyjaszewski and coworkers.[47] In contrast with disperse side chain samples, sharp transitions were consistently observed for all discrete bottlebrush polymer samples (**PBB-2, PBB-4, and PBB-8**), which reinforces the importance of discrete side chains in illuminating properties not seen in conventional disperse side chain systems. Because all samples

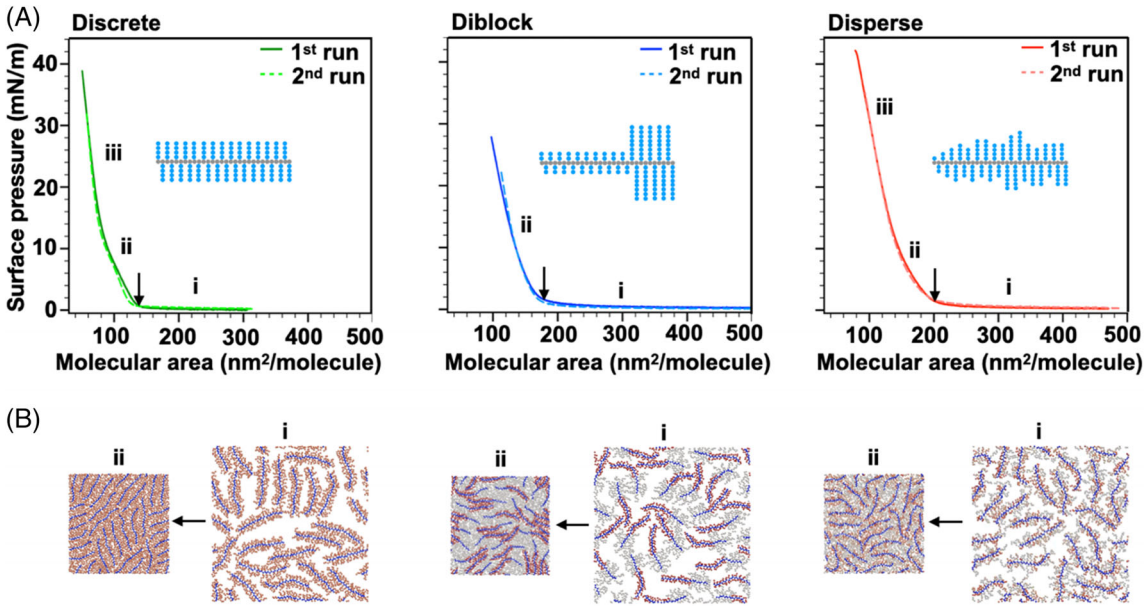

FIGURE 3 (A) Langmuir–Blodgett isotherms of discrete (green), artificial blend of dimer-octamer (blue), and disperse (red) side chain containing bottlebrush polymers. Phases corresponding to gaseous, liquid-expanded, and liquid-condensed are labeled with i, ii, and iii, respectively. Black arrows indicate the onset of surface pressure increase. (B) Coarse-grained molecular dynamic simulation snapshots of closely packed bottlebrush polymers upon a theoretical compression at ~100 nm^2/molecule. The polymer backbone is colored in blue, while the side chains are colored on a gradient from red (dimer) to white (octamer)

have non-polar polynorbornene backbones and slightly polar oligo(tBA) side chains (anisotropic monomer orientations), multi-layer growth upon compression is unlikely to occur, at least under the given compression factor.

We found that the onset of surface pressure increase for the discrete side chain bottlebrush occurs at significantly lower compressed area per molecule compared to their disperse or diblock counterparts. This result suggests that bottlebrush polymers with discrete side chains can accommodate closer packing than their disperse side chain counterparts, while exhibiting previously unseen sharp transitions from gaseous to liquid-expanded and then to liquid-condensed phases. The presence of higher molecular weight side chains impacts the onset of surface pressure toward regime 'ii', as seen through comparing the isotherm profiles for BB-4 and PBB-4 (195 and 132 nm^2/molecule), including those of **PBB-2**, **PBB-4**, and **PBB-8** (Figure S7, 105, 132, and 225 nm^2/molecule, respectively). In addition, we confirmed that the isotherms for discrete side chain bottlebrushes display three different regimes, suggesting that even bottlebrush polymers with discrete short side chains like **PBB-2** exhibit bottlebrush-like behavior.

The simulated Langmuir–Blodgett style isotherms were calculated as described in section 2.7 and presented in Figure S8. Videos of each of the three simulations can be found in the Supporting Information. Video S1 shows the diblock bottlebrush, video S2 shows the discrete sidechain bottlebrush, and video S3 shows the disperse side chain bottlebrush.While the model results are less distinct, the experimental and simulated results qualitatively match. The discrete tetramer side chain bottlebrush surface pressure rises at the largest area/molecule value, followed by the blend of discrete dimer and octamer side chain bottlebrush and then the disperse tetramer side chain bottlebrush. Experimental and modeled results also agree that the discrete side chain bottlebrush monolayer surface pressure rises more rapidly upon compression, followed by blended dimer/octamer side chain bottlebrush and then the disperse tetramer side chain bottlebrush. The simulations show that the discrete side chains give rise to straight backbones with highly uniform, locally ordered backbone spacing. In comparison, the disperse sample shows a large range of backbone spacings and lower persistence length (Figure 3B and videos in SI). The diblock sample appears between both aspects. This conjecture is further supported by the pair distribution function plotted in Figure S10 where the discrete side chain bottlebrush shows a distinct peak at ~7 (4.2 nm), corresponding to the average distance between two backbones, and the diblock shows a peak around 4.4 (2.63 nm), corresponding to the distance between two backbones with dimer side chains. The disperse side chain bottlebrush shows no obvious peak at higher r.

Interestingly, it appears from visual inspections that the diblock close-packed simulation shows some preference for aggregation of like chain lengths. This is supported by the peak correlated to the interbackbone

distance with dimer side chains in the pair-distribution function shown in Figure S10. While a deeper study into the shapes taken by the molecules under pressure and the aggregation of different side-chain lengths is warranted, it may be caused by the asymmetric shape of the diblock bottlebrush samples (each brush contains ~20 dimer and ~10 octamer repeat units). It is reasonable to expect that the interbrush interactions between octamer and dimer blocks would be favorable for closing the gaps between the brushes, but this would require significant backbone bending. While this bending would be required to closely pack the bottlebrushes, this is energetically unfavorable, and we speculate that the packed structure favors the interaction between 'excess' dimer blocks, which is more energetically favorable than a severe backbone bending.

This simulated data explains some of the features seen in the experimental results; specifically, the very sharp and clear increase in surface pressure for the discrete side chain bottlebrush sample (Figure 3A). The discrete side chains can form dense, neatly packed structures at the interface, so little increase in surface pressure is seen until relatively small areas where a sharp increase is observed. This can be said across all three discrete samples (dimer, tetramer, and octamer).

However, there are differences between the simulation and experiment. The differences between the modeled results do not show a second slope change. This deviation is likely due to the restricted two-dimensional nature of these simple simulations. Such a restriction prevents any three-dimensional perturbation of the molecules such as overlapping, reconfiguration of the side chains away from the interface, or interdigitation. At very high pressure, these conformational changes are likely to occur and are responsible for the three different observed surface pressure slopes. Full 3D simulations of these experiments with explicit air-water interfaces are warranted to investigate these kinds of rearrangement and the effects of discrete side chains. Additionally, the differences between the simulated discrete, diblock, and disperse bottlebrushes are smaller than those found experimentally. This may be caused by the lack of backbone dispersity included in the model, or the lack of fully realized polymer/water or polymer/air interactions, both of which are well suited to be considered in future works.

4 | CONCLUSIONS

We have demonstrated that the dispersity of side chains plays an important role in regulating the assembly behavior of bottlebrush polymers at the air-water interface through the synthesis of bottlebrush polymers with disperse, discrete, and diblock side chain architectures. Notably, bottlebrushes with discrete side chains achieve a higher packing density and exhibit previously unknown distinct phase transitions, which are unseen in their disperse counterparts. Furthermore, the improved topological precision from discrete side chains allowed us to discover the impact of side chain length on the Langmuir–Blodgett isotherms of bottlebrush polymers. With experimental findings corroborated by coarse-grained molecular dynamics simulations, such shape-defined bottlebrush polymers offer exciting opportunities to advance structure–property relationship studies of branched polymers and provide new design rules for engineering soft materials at the molecular level for emerging precision technologies.

ACKNOWLEDGMENTS

This work was supported by the LSU start-up funding, BASF Living Sustainability Laboratory Program, and Louisiana Board of Regents funding (RD-A-07, Jimmy Lawrence, Nduka D. Ogbonna). Bhuvnesh Bharti acknowledges the support from NSF (CBET-2038305), and Andrew Peters acknowledges the support from Louisiana Tech start-up funding, and Louisiana Board of Regents funding (RD-A-18). The authors acknowledge the support for material characterizations by the NMR, Polymer Analysis Laboratory, and Shared Instrumentation Facilities at Louisiana State University. The authors acknowledge the helpful discussion and technical support from Japan Analytical Industry (JAI). The high-performance computing resources provided by the Louisiana Optical Network Infrastructure (https://loni.org) were used for this work.

DATA AVAILABILITY STATEMENT

The data that support the findings of this study are available from the corresponding authors.

ORCID

Nduka D. Ogbonna https://orcid.org/0000-0001-9383-6023
Andrew J. Peters https://orcid.org/0000-0001-5031-2828
Jimmy Lawrence https://orcid.org/0000-0003-4455-6177

REFERENCES

[1] J. Yang, I. Gitlin, V. M. Krishnamurthy, J. A. Vazquez, C. E. Costello, G. M. Whitesides, *J. Am. Chem. Soc.* **2003**, *125*, 12392.
[2] J. Zhang, J. S. Moore, Z. Xu, R. A. Aguirre, *J. Am. Chem. Soc.* **1992**, *114*, 2273.
[3] L. Hartmann, H. G. Börner, *Adv. Mater.* **2009**, *21*, 3425.
[4] J. M. Tour, *Chem. Rev.* **1996**, *96*, 537.
[5] D. Schaffert, E. Wagner, *Gene Ther.* **2008**, *15*, 1131.

[6] E. Kumarasamy, S. N. Sanders, A. B. Pun, S. A. Vaselabadi, J. Z. Low, M. Y. Sfeir, M. L. Steigerwald, G. E. Stein, L. M. Campos, *Macromolecules* **2016**, *49*, 1279.
[7] L. Zhang, N. S. Colella, F. Liu, S. Trahan, J. K. Baral, H. Henning Winter, S. C. B. Mannsfeld, A. L. Briseno, *J. Am. Chem. Soc.* **2013**, *135*, 844.
[8] C. J. Hawker, E. E. Malmström, C. W. Frank, J. P. Kampf, *J. Am. Chem. Soc.* **1997**, *119*, 9903.
[9] M. B. Koo, S. W. Lee, J. M. Lee, K. T. Kim, *J. Am. Chem. Soc.* **2020**, *142*, 14028.
[10] K. Takizawa, C. Tang, C. J. Hawker, *J. Am. Chem. Soc.* **2008**, *130*, 1718.
[11] J. Lawrence, S.-H. Lee, A. Abdilla, M. D. Nothling, J. M. Ren, A. S. Knight, C. Fleischmann, Y. Li, A. S. Abrams, B. V. K. J. Schmidt, M. C. Hawker, L. A. Connal, A. J. McGrath, P. G. Clark, W. R. Gutekunst, C. J. Hawker, *J. Am. Chem. Soc.* **2016**, *138*, 6306.
[12] Y. Jiang, M. R. Golder, H. V.-T. Nguyen, Y. Wang, M. Zhong, J. C. Barnes, D. J. C. Ehrlich, J. A. Johnson, *J. Am. Chem. Soc.* **2016**, *138*, 9369.
[13] J. Lawrence, E. Goto, J. M. Ren, B. McDearmon, D. S. Kim, Y. Ochiai, P. G. Clark, D. Laitar, T. Higashihara, C. J. Hawker, *J. Am. Chem. Soc.* **2017**, *139*, 13735.
[14] W. R. Gutekunst, C. J. Hawker, *J. Am. Chem. Soc.* **2015**, *137*, 8038.
[15] M. E. J. Vleugels, M. E. de Zwart, J. R. Magana, B. A. G. Lamers, I. K. Voets, E. W. Meijer, K. Petkau-Milroy, A. R. A. Palmans, *Polym. Chem.* **2020**, *11*, 7170.
[16] A. Das, K. Petkau-Milroy, G. Klerks, B. Van Genabeek, R. P. M. Lafleur, A. R. A. Palmans, E. W. Meijer, *ACS Macro Lett.* **2018**, *7*, 546.
[17] J. De Neve, J. J. Haven, S. Harrisson, T. Junkers, *Angew. Chem. Int. Ed Engl.* **2019**, *58*, 13869.
[18] E. M. Timmers, P. M. Fransen, Á. González García, S. M. C. Schoenmakers, J. R. Magana, J. W. Peeters, R. Tennebroek, I. van Casteren, R. Tuinier, H. M. Janssen, I. K. Voets, *Polym. Chem.* **2021**, *12*, 2891.
[19] J. C. Barnes, D. J. C. Ehrlich, A. X. Gao, F. A. Leibfarth, Y. Jiang, E. Zhou, T. F. Jamison, J. A. Johnson, *Nat. Chem.* **2015**, *7*, 810.
[20] S. E. Seo, C. J. Hawker, *Macromolecules* **2020**, *53*, 3257.
[21] D. A. Tomalia, H. Baker, J. Dewald, M. Hall, G. Kallos, S. Martin, J. Roeck, J. Ryder, P. Smith, *Macromolecules* **1986**, *19*, 2466.
[22] Y. H. Kim, O. W. Webster, *Macromolecules* **1992**, *25*, 5561.
[23] R. Verduzco, X. Li, S. L. Pesek, G. E. Stein, *Chem. Soc. Rev.* **2015**, *44*, 2405.
[24] M. Wintermantel, M. Gerle, K. Fischer, M. Schmidt, I. Wataoka, H. Urakawa, K. Kajiwara, Y. Tsukahara, *Macromolecules* **1996**, *29*, 978.
[25] Y. Nakamura, T. Norisuye, *Polym. J.* **2001**, *33*, 874.
[26] J. M. Sarapas, T. B. Martin, A. Chremos, J. F. Douglas, K. L. Beers, *Proc. Natl. Acad. Sci. U. S. A.* **2020**, *117*, 5168.
[27] Y. Xia, J. A. Kornfield, R. H. Grubbs, *Macromolecules* **2009**, *42*, 3761.
[28] R. H. G. Brinkhuis, A. J. Schouten, *Macromolecules* **1991**, *24*, 1487.
[29] W.-P. Hsu, Y.-L. Lee, S.-H. Liou, *Appl. Surf. Sci.* **2006**, *252*, 4312.
[30] C. Zhang, D. S. Kim, J. Lawrence, C. J. Hawker, *ACS Macro Lett.* **2018**, *7*, 921.
[31] M. S. Sanford, J. A. Love, R. H. Grubbs, *Organometallics* **2001**, *20*, 5314.
[32] V. Percec, T. Guliashvili, J. S. Ladislaw, A. Wistrand, A. Stjerndahl, M. J. Sienkowska, M. J. Monteiro, S. Sahoo, *J. Am. Chem. Soc.* **2006**, *128*, 14156.
[33] D. J. Lunn, S. Seo, S.-H. Lee, R. B. Zerdan, K. M. Mattson, N. J. Treat, A. J. McGrath, W. R. Gutekunst, J. Lawrence, A. Abdilla, A. Anastasaki, A. S. Knight, B. V. K. J. Schmidt, M. W. Bates, P. G. Clark, J. P. DeRocher, A. K. Van Dyk, C. J. Hawker, *J. Polym. Sci., Part A: Polym. Chem.* **2019**, *57*, 716.
[34] S. C. Radzinski, J. C. Foster, S. J. Scannelli, J. R. Weaver, K. J. Arrington, J. B. Matson, *ACS Macro Lett.* **2017**, *6*, 1175.
[35] L. Zhao, M. Byun, J. Rzayev, Z. Lin, *Macromolecules* **2009**, *42*, 9027.
[36] Y. Seo, J.-H. Im, J.-S. Lee, J.-H. Kim, *Macromolecules* **2001**, *34*, 4842.
[37] K. Kremer, G. S. Grest, *J. Chem. Phys.* **1990**, *92*, 5057.
[38] M. L. Miller, C. E. Rauhut, *J. Polym. Sci.* **1959**, *38*, 63.
[39] J. A. Anderson, J. Glaser, S. C. Glotzer, *Comput. Mater. Sci.* **2020**, *173*, 109363.
[40] J. Glaser, T. D. Nguyen, J. A. Anderson, P. Lui, F. Spiga, J. A. Millan, D. C. Morse, S. C. Glotzer, *Comput. Phys. Commun.* **2015**, *192*, 97.
[41] V. Matlab, Natick, MA, USA: MathWorks Inc **2018**.
[42] Y. Xia, B. D. Olsen, J. A. Kornfield, R. H. Grubbs, *J. Am. Chem. Soc.* **2009**, *131*, 18525.
[43] L. Zhao, M. D. Goodman, N. B. Bowden, Z. Lin, *Soft Matter* **2009**, *5*, 23.
[44] I. I. Perepichka, Q. Lu, A. Badia, C. G. Bazuin, *Langmuir* **2013**, *29*, 4502.
[45] M. Choi, B. Chung, B. Chun, T. Chang, *Macromol. Res.* **2004**, *12*, 127.
[46] A. Al Harraq, B. Bharti, *Soft Matter* **2020**, *16*, 9643.
[47] J. Burdyńska, W. Daniel, Y. Li, B. Robertson, S. S. Sheiko, K. Matyjaszewski, *Macromolecules* **2015**, *48*, 4813.
[48] S. A. Evenson, J. P. S. Badyal, C. Pearson, M. C. Petty, *J. Phys. Chem.* **1996**, *100*, 11672.

SUPPORTING INFORMATION

Additional supporting information may be found in the online version of the article at the publisher's website.

How to cite this article: N. D. Ogbonna, M. Dearman, B. Bharti, A. J. Peters, J. Lawrence, *J. Polym. Sci.* **2021**, *59*(21), 2458. https://doi.org/10.1002/pol.20210565